Polarity Effects on ZnO Films Grown along the Nonpolar $[11\bar{2}0]$ Direction

Jesús Zúñiga-Pérez and Vicente Muñoz-Sanjosé
Departament Física Aplicada i Electromagnetisme, Universitat de València, C/Dr. Moliner 50, 46100 Burjassot, Spain

Elisa Palacios-Lidón and Jaime Colchero
Departamento de Física, Facultad de Química, Campus Espinardo, Universidad de Murcia, 30100 Murcia, Spain
(Received 8 August 2005; published 22 November 2005)

The surface electrical properties of ZnO thin films grown along the nonpolar $[11\bar{2}0]$ direction have been investigated by Kelvin probe microscopy on a nanometer scale. Two different charge domains, with a 75 meV work function difference, coexist within the ZnO surface, which is covered by rhombohedral pyramids whose sidewalls are shown to be $\{10\bar{1}1\}$-type planes. The presence and relative orientation of the two kinds of charge domains are explained in terms of the atomic arrangement at the $\{10\bar{1}1\}$ polar surfaces.

DOI: 10.1103/PhysRevLett.95.226105 PACS numbers: 68.47.Gh, 68.37.−d, 73.30.+y, 73.63.−b

Metal oxides surfaces have attracted a lot of interest in recent years due to their unique stability properties as well as their use in technologically important domains such as optoelectronics, spintronics, and catalysis. From a fundamental point of view, polar oxide surfaces should present a nonvanishing electrostatic dipole moment perpendicular to the surface that would make them unstable. However, numerous polar oxides surfaces have been shown to be stable and different mechanisms leading to the dipole cancellation have been established [1]. In particular, the basal O-$(000\bar{1})$ and Zn-(0001) planes of wurtzite ZnO, whose structure consists of alternating hexagonal Zn and O planes stacked along the [0001] axis, have been studied both experimentally [2–7] and theoretically [3,5,8]. Charge transfer from the O-$(000\bar{1})$ to the Zn-(0001) surface [3,8], hydrogen adsorption on the Zn-(0001) [9] and O-$(000\bar{1})$ faces [10], and removal of Zn atoms from the Zn-terminated face [5] have been found to stabilize the polar ZnO(0001) and ZnO$(000\bar{1})$ surfaces.

The surface stabilization mechanisms that quench the macroscopic electrostatic field in an isolated crystal may be perturbed or hindered if additional material is deposited on top, as required by quantum heterostructures exploited in the optoelectronic industry. Devices based on [0001] wurtzite materials are known to present electrostatic fields that spatially separate electrons and holes in the active layers [11] and thus limit the device efficiency. The observed fields are due not only to the inherently polar character of the growth direction, but also to the piezoelectric effect that affects strained wurtzite layers. To overcome the detrimental effects of these electrostatic fields the growth along nonpolar directions, such as $[11\bar{2}0]$ (*a* plane) or $[10\bar{1}0]$ (*m* plane), has been proposed [12]. Among all the studied polar and nonpolar ZnO surfaces, theoretical calculations agree that $(10\bar{1}0)$ is the most stable, with a computed cleavage energy of the order of 2 J/m^2 [6,8,13]. This stability may be at the origin of the surface flatness observed by scanning tunneling microscopy (STM) [4,6]. On the other hand, the cleavage energy of the nonpolar ZnO$(11\bar{2}0)$ surface, whose structure consists of ZnO dimers running along [0001], is still controversial. The computed ZnO$(11\bar{2}0)$ cleavage energies depend on the particular approximations and functionals employed in the evaluation [6], with local-density approximation and generalized-gradient approximation functionals leading to cleavage energies slightly higher than $(10\bar{1}0)$ [8], and B3LYP functional giving cleavage energies even higher than those of the Zn-(0001)/O-$(000\bar{1})$ system [14]. STM studies revealed that as-grown $(11\bar{2}0)$ surfaces on vapor transport samples were covered by grooves running parallel to $[1\bar{1}00]$ whose sides were limited by $\pm(0001)$ planes [4]. These rough surfaces suggest a high cleavage energy. In this Letter scanning force microscopy (SFM) techniques—SFM "nanogoniometry" and Kelvin probe microscopy (KPM)—are used to characterize in detail the morphology and the electrical properties of faceted ZnO thin films grown along the nonpolar $[11\bar{2}0]$ direction. A direct relationship between the surface electrical properties and the polar character of the facets will be established.

SFM nanogoniometry [15] was performed to determine the orientation of the ZnO surface facets. In order to obtain a complete statistical description of the facets' orientation, topographic images are processed following a new methodology: first, the local normal vector is calculated at each point of the image; then, an orientation histogram is constructed with all these normal vectors. The height of each peak is a direct measurement of the statistical weight of the corresponding facet orientation. For samples showing well-defined facets the orientation histogram shows distinct peaks corresponding to each of the orientations present in the topographic image.

KPM [16] is used to measure the contact potential locally. KPM works by applying an adjustable bias voltage $U_{\mathrm{bias}}(t) = U_{\mathrm{tip}} + U_{\mathrm{ac}}\sin(\omega_e t)$ between a conducting tip and the sample. Since the electrostatic interaction is quadratic in the voltage, $V(z) = C(z)(U_{\mathrm{bias}} - U_{\mathrm{CP}})^2/2$, with $C(z)$ the tip-sample capacitance and U_{CP} the contact potential of the sample with respect to the tip, the measured interaction has

a static component and two others varying with frequencies ω_e and $2\omega_e$. Using appropriate lock-in techniques and a feedback loop to adjust the tip-sample voltage, the local contact potential can be determined with nanometer resolution. All measurements described here were performed using the frequency shift (force gradient) as the signal source [17], since this method leads to improved signal-to-noise ratio and higher spatial resolution [18]. A relatively small modulation bias of $U_{\mathrm{ac}} = 500$ mV at a resonance frequency of 7 kHz was used in order to avoid band bending effects. To further improve the signal-to-noise ratio and to avoid spurious tip-sample interactions appearing in the electrostatic signal, data were acquired in a ''retrace scan mode.'' For each image line, first a topography scan is obtained by maintaining a certain oscillation amplitude of the cantilever, typically 10% less than the free resonance amplitude $a_0 (a_0 \approx 5\,\mathrm{nm}_{pp})$; then, the tip is lifted 4 nm over the measured topography and a second scan is made in the ''Kelvin method'' to obtain the contact potential of the sample. During this second scan, the cantilever oscillation amplitude is equal to the free resonance amplitude, and therefore the tip is in the ''true'' noncontact regime.

ZnO thin films were grown by metal-organic vapor phase epitaxy on $(01\bar{1}2)$ *r*-plane sapphire substrates under oxygen-rich conditions at a temperature of 376 °C. X-ray $\theta/2\theta$ scans show that the growth direction, that is, the surface normal, is parallel to $[11\bar{2}0]$. In the initial growth stages the films morphology is induced by the atomic step structure of the *r*-plane sapphire substrate [19]. As thickness increases, facets gradually develop on the surface. The morphology of the latter samples [Fig. 1(a)] consists of rhombohedral-base pyramids, which are connected along their elongation axis forming continuous grains some micrometers long. The sidewalls of the pyramids are the focus of the present study. The orientation of these sidewalls can be determined by SFM nanogoniometry. The corresponding orientation histogram is shown in Fig. 1(b) and indicates that the facets form $40° \pm 2°$ with respect to the growth direction. In order to identify the morphological facets with crystallographic planes, the distribution of topographic normals must be compared with the stereographic projection corresponding to $(11\bar{2}0)$-oriented ZnO. In this way, it has been possible to associate particular Miller index with the pyramids faces, which have been found to belong to the $\{10\bar{1}1\}$ family. The measured value matches the calculated angle between the $\{10\bar{1}1\}$ family and the $(11\bar{2}0)$ plane, which is 40.37°. Since only four peaks are detected in Fig. 2(b), and, in particular, no central peak corresponding to the nonpolar ZnO$(11\bar{2}0)$ plane is found, we conclude that the whole sample is covered by $\{10\bar{1}1\}$-type planes. Figure 1(c) shows the experimental pole figure of ZnO $\{10\bar{1}1\}$ reflections, which reproduces the symmetry of the facets orientation shown in Fig. 1(b) and thus confirms the $\{10\bar{1}1\}$ ascription. Furthermore, from

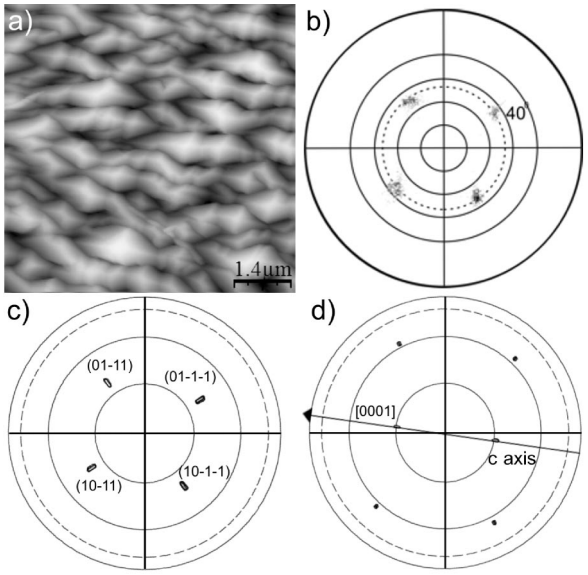

FIG. 1. (a) Topography image of the ZnO surface. (b) Calculated topographic normals distribution. Experimental pole figures of (c) ZnO$\{10\bar{1}1\}$ reflections and (d) ZnO$\{11\bar{2}1\}$ reflections.

the ZnO $\{11\bar{2}1\}$ pole figure [Fig. 1(d)] the polar ZnO $[0001]$ axis is seen to be parallel to the pyramids longest axis, indicating that the stripes seen in Fig. 1(a) are aligned along the $[0001]$ axis. The faceting of the growing $(11\bar{2}0)$ surface supports the theoretical calculations that assign it a high cleavage energy and would be compatible with a lower cleavage energy for the $\{10\bar{1}1\}$ planes. In ZnO these planes had been previously detected in nanostructures, inducing the growth of ZnO nanofingers and determining the growth of deformation-free single crystal nanohelixes [20], and in hydrothermally grown single crystals [21].

Figures 2(a) and 2(b) show topographic and contact potential images of the same surface area. In Fig. 2(b) bright and dark regions, associated with higher and lower contact potential areas, respectively, appear. Differences in the contact potential can be associated with variations of the surface charge density. These regions with constant surface charge density will be referred to, from now on, as ''charge domains.'' From the comparison of both images, a clear correlation between morphological facets and contact potential is established, with different charge domains alternating along the $[0001]$ axis. Although the four facets belong to the same crystallographic family, $\{10\bar{1}1\}$, we have found that they are not electrically equivalent. In Fig. 2(c) the surface contact potential distribution measured inside the solid square in Fig. 2(b) is represented. This distribution, obtained from a $2.5 \times 2.5\ \mu\mathrm{m}^2$ area containing several charge domains, shows only two peaks centered at about $+30$ and -45 mV with respect to the mean contact potential of the total image. Hence, only two types of charge domains with an average contact potential difference of 75 mV are present in the sample. The widths

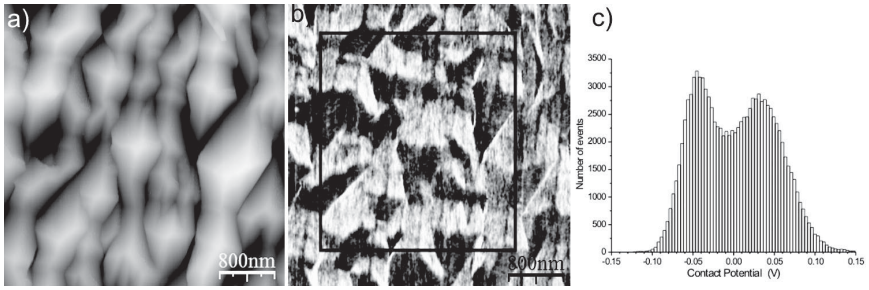

FIG. 2. (a) Topography and (b) surface contact potential images of the ZnO surface. (c) Contact potential distribution measured inside the solid square shown in (b).

of the peaks are due to border effects and/or sample inhomogeneities rather than to the intrinsic error of the technique ($\lesssim$10 mV). The obtained values are consistent with contact potential differences measured in related wurtzite materials (GaN) [22]. A single pyramid, shown in Figs. 3(a) and 3(b), has been monitored in order to correlate the orientation of the charge domains with respect to the ZnO [0001] axis. Comparing topography and surface contact potential line profiles measured parallel and perpendicular to the c axis [Figs. 3(c) and 3(d), respectively], we find that the contact potential only changes when crossing from one facet to the other along the [0001] direction.

The fact that different charge domains alternate along the [0001] axis points towards a polarity effect related with the surface atomic structure of the $\{10\bar{1}1\}$ planes. The way in which these planes intersect the [0001] axis is depicted in Fig. 4(a). The construction illustrates how the pyramids facets grow along the $[11\bar{2}0]$ direction. In Fig. 4(b), the structure is viewed along the $[\bar{1}2\bar{1}0]$ direction, which is the direction determined by the intersection of planes $(10\bar{1}1)$ and $(10\bar{1}\,\bar{1})$. While the surface facing the positive [0001] axis contains only zinc ions, the opposing surface contains a topmost atomic plane covered exclusively by oxygen ions, leading to opposite polarities. In the KPM images, the Zn-rich facet would give a bright contrast, whereas the O-rich facet would result in a darker contrast, as seen in Figs. 2(b) and 3(b). If we consider facets joined along $\langle 11\bar{2}\,\bar{3}\rangle$-type edges [Fig. 4(c)], the predominating surface ions, and their surface density, are the same at both sides of the edge, implying that no change should be appreciated in the contact potential. KPM can thus be used to unambiguously determine the direction of the [0001] axis in terms of polarity and overcome some of the difficulties encountered in convergent beam electron diffraction.

All the images obtained on this sample discard the presence of inversion domain boundaries (IDBs) at this spatial scale. If IDBs were present, charge domains equally charged (positively or negatively) and pertaining to different pyramids should be in contact along the IDB. However, as we move along [0001] from one pyramid to the adjacent one the sign of the charge domains always changes, thus maintaining the alternating charge sign series, $(+\,-\,+\,-\cdots)$, as required by an IDBs-free sample.

The described faceting tends to expose polar surfaces which are accompanied by electrostatics fields that would decrease device efficiency. This result highlights that growth along nonpolar directions is not sufficient to obtain heterostructures free of electrostatic fields: in addition, faceting into polar surfaces must be prevented. When this

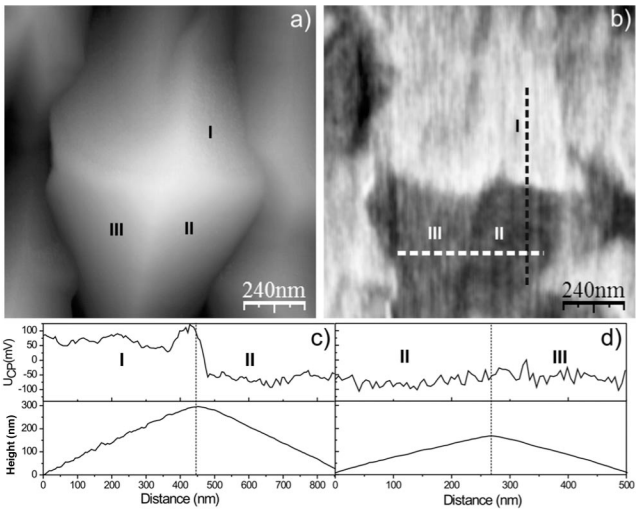

FIG. 3. (a) Topography and (b) surface contact potential images of a single pyramid. Topography and surface contact potential line scans measured (c) parallel and (d) perpendicular to the [0001] direction.

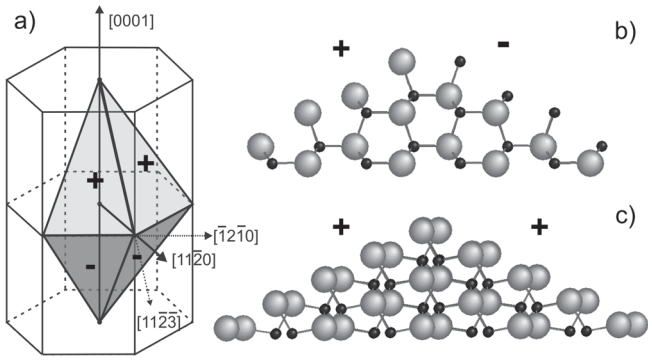

FIG. 4. (a) Schematic representation of $\{10\bar{1}1\}$ facets in the wurtzite structure. Atomic model of the $\{10\bar{1}1\}$ facets projected along (b) the $[\bar{1}2\bar{1}0]$ direction and (c) the $[11\bar{2}\,\bar{3}]$ direction. Large spheres represent zinc atoms, small spheres oxygen atoms.

faceting occurs the surface becomes electrically inhomogeneous, exposing regions with different work functions that affect the transport properties across the surface. Spatial fluctuations of the barrier height in a Schottky contact were modeled by introducing a barrier distribution characterized by a mean barrier height and a standard deviation [23]. Within this formalism, ideality factors larger than 1 and barrier heights values dependent on the measurement technique employed, current/voltage or capacitance/voltage, are just a consequence of the potential fluctuations. Ag Schottky contacts on $(11\bar{2}0)$-oriented ZnO have shown ideality factors around 1.33 [24], while a recent study of Schottky contacts on (0001)-oriented ZnO thin films [25] has found that a standard deviation of the barrier distribution of 134 ± 10 meV could account for the measured transport characteristics. We note that in $(11\bar{2}0)$-oriented ZnO films displaying $\{10\bar{1}1\}$ facets, the barrier distribution, if no additional potential fluctuations were considered, would mimic the work function distribution shown in Fig. 2(c). Rather than having one barrier height distribution, we would have two barrier height distributions separated by 75 meV. Similar effects should be also expected in the most commonly used ZnO (0001)-oriented films, where polar {0001} and nonpolar $\{10\bar{1}0\}$ surfaces are exposed simultaneously due to columnar growth along [0001].

In summary, the actual study demonstrates the potential of KPM to study polarity effects and, in general, electrostatic properties of metal oxides surfaces on a nanometer scale. In particular, the presence of opposite charge domains on faceted ZnO$(11\bar{2}0)$ thin films has been established, with rhombohedral pyramids covering the ZnO surface and exposing polar $\{10\bar{1}1\}$ facets. Opposite polarity domains alternate along the in-plane [0001] axis, as expected from the atomic structure of the facets, with no IDB being detected. The implications of charge domains coexistence on technological important issues, such as quantum heterostructures efficiency and Schottky contacts homogeneity, have been discussed. Another important field where ZnO plays a fundamental role is heterogeneous catalysis, especially in the synthesis of methanol. Because the catalytic active sites depend on the particular surface atomic arrangements, $\{10\bar{1}1\}$ polar surfaces could provide new adsorption sites to be exploited.

We acknowledge enlightening discussions with H. von Wenckstern and support from B. Pérez, J. Abellán, and A. Urbina. This work was supported by the Spanish government under projects MAT2002-01084, MAT2004-06841, GV-Grupos 03/098, SOXESS European Network, and the Fundación Séneca-CARM.

[1] C. Noguera, J. Phys. Condens. Matter **12**, R367 (2000).
[2] N. Jedrecy, M. Sauvage-Simkin, and R. Pinchaux, Appl. Surf. Sci. **162–163**, 69 (2000).
[3] A. Wander, F. Schedin, P. Steadman, A. Norris, R. McGrath, T. S. Turner, G. Thornton, and N. M. Harrison, Phys. Rev. Lett. **86**, 3811 (2001).
[4] O. Dulub, L. A. Boatner, and U. Diebold, Surf. Sci. **519**, 201 (2002).
[5] O. Dulub, U. Diebold, and G. Kresse, Phys. Rev. Lett. **90**, 016102 (2003).
[6] U. Diebold, L. V. Koplitz, and O. Dulub, Appl. Surf. Sci. **237**, 336 (2004).
[7] A. Wander and N. M. Harrison, J. Chem. Phys. **115**, 2312 (2001); G. Kresse, O. Dulub, and U. Diebold, Phys. Rev. B **68**, 245409 (2003).
[8] B. Meyer and D. Marx, Phys. Rev. B **67**, 035403 (2003).
[9] M. Losurdo and M. M. Giangregorio, Appl. Phys. Lett. **86**, 091901 (2005).
[10] M. Kunat, St. Gil Girol, Th. Becker, U. Burghaus, and Ch. Wöll, Phys. Rev. B **66**, 081402 (2002); V. Staemmler, D. Marx, M. Kunat, S. Gil Girol, U. Burghaus, and Ch. Wöll, Phys. Rev. Lett. **90**, 106102 (2003); B. Meyer, Phys. Rev. B **69**, 045416 (2004).
[11] M. Leroux, O. Brandt, N. Grandjean, M. Laügt, J. Massies, B. Gil, P. Lefebvre, and P. Bigenwald, Phys. Rev. B **58**, R13371 (1998).
[12] P. Waltereit, O. Brandt, A. Trampert, H. T. Grahn, J. Menniger, M. Ramsteiner, M. Reiche, and K. H. Ploog, Nature (London) **406**, 865 (2000).
[13] A. Wander and N. M. Harrison, Surf. Sci. **457**, L342 (2000).
[14] A. Wander and N. M. Harrison, Surf. Sci. **468**, L851 (2000).
[15] E. Palacios-Lidón, J. Zúñiga-Pérez, V. Muñoz-Sanjosé, and J. Colchero (unpublished).
[16] J. M. R. Weaver and D. W. Abraham, J. Vac. Sci. Technol. B **9**, 1559 (1991); M. Nonnenmacher, M. P. ÓBoyle, and H. K. Wickramasinghe, Appl. Phys. Lett. **58**, 2921 (1991).
[17] E. Palacios-Lidón, J. F. Abellán, J. Colchero, C. Munuera, and C. Ocal, Appl. Phys. Lett. **87**, 154106 (2005).
[18] J. Colchero, A. Gil, and A. M. Baró, Phys. Rev. B **64**, 245403 (2001); L. C. Lei, A. Das, M. Elliott, and J. E. Macdonald, Nanotechnology **15**, 627 (2004); U. Zerweck, C. Loppacher, T. Otto, S. Grafström, and L. M. Eng, Phys. Rev. B **71**, 125424 (2005).
[19] C Munuera, J. Zúñiga-Pérez, J. F. Rommeluere, V. Sallet, R. Triboulet, V. Muñoz-Sanjosé, and C. Ocal, J. Cryst. Growth **264**, 70 (2004).
[20] Z. L. Wang, X. Y. Kong, and J. M. Zuo, Phys. Rev. Lett. **91**, 185502 (2003); R. Yang, Y. Ding, and Z. L. Wang, Nano Lett. **4**, 1309 (2004).
[21] T. Sekiguchi, S. Miyashita, K. Obara, T. Shishido, and N. Sakagami, J. Cryst. Growth **214–215**, 72 (2000).
[22] K. M. Jones, P. Visconti, F. Yun, A. A. Baski, and H. Morkoç, Appl. Phys. Lett. **78**, 2497 (2001).
[23] J. H. Werner and H. H. Güttler, J. Appl. Phys. **69**, 1522 (1991).
[24] H. Sheng, S. Muthukumar, N. W. Emanetoglu, and Y. Lu, Appl. Phys. Lett. **80**, 2132 (2002).
[25] H. von Wenckstern, G. Biehne, R. Abdel Rahman, H. Hochmuth, M. Lorenz, and M. Grundmann (unpublished); H. von Wenckstern (private communication).